Excitonic lifetimes and optical response of carbon nanotubes modulated by electrostatic gating

Mads L. Trolle and Thomas G. Pedersen

Department of Physics and Nanotechnology, Aalborg University, Skjernvej 4A, DK-9220 Aalborg East, Denmark

We investigate the excitonic optical properties of carbon nanotubes modulated by an electrostatic field applied in a direction transversal to the carbon nanotubes' axis. We find that excitation energies are redshifted while absorption peaks split due to symmetry breaking. Furthermore, from analysis of the electron-hole wave function calculated in the Wannier approximation, it is seen that the exciton wave function tends to polarize, with a separation of the electron and hole in the large-field limit. This has the effect of reducing the excitonic intrinsic radiative decay rates due to reduced electron-hole overlap. We compute thermalized effective decay rates for comparison with experiments, reflecting the interplay between exciton energy shifts and reduced intrinsic decay rates. Hence, these results suggest several possibilities for modulating the optical response of carbon nanotubes by the application of an electrostatic field in gatelike configurations.

I. INTRODUCTION

In the past decade, a great deal of attention has been devoted to uncovering the remarkable optical properties of carbon nanotubes (CNTs) [1–17]. Even with attention shifting to a new breed of two-dimensional materials perhaps better suited for realizing devices on an industrial scale [18], CNTs remain of tremendous importance for the study of low-dimensional electronic systems. The optical response of CNTs is, in the visible energy range, dominated by excitations of correlated electron-hole pairs termed excitons. [3–5,11] In low-dimensional systems, the spatial extent of these complexes is confined in at least one dimension, enhancing the attractive Coulomb interaction often resulting in exciton binding energies of several hundred meVs. The absorption spectrum has been investigated theoretically using several models, both in the independent particle approximation [8,15] and including electron-hole interaction [5,19], and measured experimentally [9,20].

Both experiments [21,22] and theory [14,16] suggest that the application of an electrostatic field across a CNT, in a direction perpendicular the tube axis, may be an effective way of tuning its optical response. This case has been considered both theoretically in the linear [1,2,10,14,15] and second harmonic [16] cases; however, all models applied to this problem have so far been at the one-electron level, neglecting important excitonic effects. It should be noted that the somewhat similar case of an electrostatic field applied parallel to the long axis of CNTs and other one-dimensional semiconductors, leading to the excitonic Franz-Keldysh effect, has been considered. [12,23]

In the present paper, we include excitons in the treatment of the optical response of several CNT species under the influence of a strong electrostatic field applied perpendicularly to their tube axes. We investigate the resulting electro-optical changes induced in the dielectric function, which should be measurable in experiments. Furthermore, we consider modulation of excitonic radiative lifetimes also of experimental relevance. In our analysis, we initially consider a simplified model of an electron-hole pair confined to the surface of a homogeneous cylinder, with an electric field applied transversally to its axis, as a model for a CNT exciton complex. While such an effective mass model has been applied before to describe

much of the fundamental physics involved [3,4], allowing, e.g., calculation of exciton binding energies, it does not contain the atomic information necessary to, for example, distinguish between various CNT chiralities, or allow the calculation of optical matrix elements. Hence, we also consider a slightly more complicated Bethe-Salpeter based model, where exciton states are expanded in a basis of singly excited, many-electron wave functions constructed from π-electron tight-binding (TB) orbitals. This method has previously been demonstrated to yield reliable results for both CNTs [5] and conjugated polymers [24].

We report that strong electrostatic fields can induce a significant splitting and redshift of the main absorption peaks in the excitonic spectrum, in addition to new features which arise from breaking optical selection rules. Many of these effects may be compared qualitatively with previous one-electron theory [1,2,10,14,15]; however, excitonic effects are of paramount importance for the prediction of correct line shapes, peak intensities, and spectral positions. Moreover, the lowest exciton states will tend to polarize upon the application of the electrostatic field, which in turn reduces the spatial overlap of electron and hole wave functions. This leads to reduced exciton radiative decay rates and, hence, increased lifetimes. To arrive at a thermalized effective decay rate for comparison with experiments [25], we perform a statistical averaging procedure [6], revealing that the observed decay rates arise from the interplay between modulated exciton decay rates and the accompanying redshifts.

In the following, the theoretical methods applied are reviewed, starting with the simple case of an electron-hole pair confined to a cylinder surface. Next, the exciton model based on a TB band structure is considered followed by the introduction of the methods for optical response and radiative recombination rate calculations.

II. THEORY AND METHODS

A. Wannier effective mass model

Similarly to Refs. [3,4,19], we model the excitonic states using a two-particle Hamiltonian, describing an electron and a hole confined to the surface of a homogeneous cylinder,

$$\hat{H}_{eh} = \hat{K} + V_{eh} + V_{ext}, \tag{1}$$

where $\hat{K}$ is the two-particle kinetic energy operator, V_{eh} is the Coulomb interaction potential between electron and hole, while V_{ext} describes the externally applied electrostatic field. Hence, exciton binding energies and wave functions are found, respectively, as eigenvalues and eigenvectors to $\hat{H}_{eh}$. Converting to effective exciton units, the electron and hole kinetic energies (in effective exciton Rydbergs Ry^*) in cylindrical coordinates may be written as [4]

$$\hat{K} = -\frac{1}{M^*}\frac{\partial^2}{\partial Z^2} - \frac{1}{\mu}\frac{\partial^2}{\partial z^2} - \frac{1}{m_e^* R^2}\frac{\partial^2}{\partial \theta_e^2} - \frac{1}{m_h^* R^2}\frac{\partial^2}{\partial \theta_h^2}. \quad (2)$$

The effective electron and hole masses (in units of the reduced electron-hole mass) are denoted m_e^* and m_h^*, while $M^* = m_e^* + m_h^*$ and $\mu = m_e^* m_h^*/(m_e^* + m_h^*)$. The CNT radius is denoted R, while z and Z are, respectively, the relative and center-of-mass axial coordinates—all in exciton Bohr radii a_B^*. Moreover, θ_e and θ_h are the angular coordinates of the electron and hole, respectively. Using these conventions, the attractive Coulomb interaction between the electron and hole V_{eh} may be written as

$$V_{eh} = -\frac{2}{\sqrt{z^2 + 4R^2 \sin^2[\theta_e/2 - \theta_h/2]}}, \quad (3)$$

while the electrostatic potential energy term V_{ext} takes the form

$$V_{ext} = FR(\cos\theta_e - \cos\theta_h), \quad (4)$$

F denoting the electrostatic field strength. The valence and conduction bands nearest to the Fermi level are dominated by π-electron states, and may be approximated fairly accurately as mirror symmetric across the Fermi level (for undoped samples). In fact, in the much-used nearest-neighbor orthogonal TB model, this is also the case [26]. Hence, we apply identical electron and hole masses $m_h^* = m_e^* = 2$, $M^* = 4$, and $\mu = 1$.

The Hamiltonian Eq. (1) is diagonalized in a suitable basis, where we take the angular behavior to be described by complex exponential functions $g_l(\theta) = 1/\sqrt{2\pi}\exp il\theta$, while the dependence on the relative axial coordinate z is taken to be Gaussian $f_n(z) = \exp(-\alpha_n z^2)$. Here, l is an integer indicating angular momentum, while α_n represents a variational parameter determining the decay of the wave function with axial electron-hole separation. Hence, the nth electron-hole wave function is expanded according to

$$\Psi_n(z, \theta_e, \theta_h) = \sum_{n=1}^{N_\alpha} \sum_{l,k=-N_k}^{N_k} C_{nkl} f_n(z) g_k(\theta_e) g_l(\theta_h), \quad (5)$$

with the parameters $\{\alpha_i\}$ determined variationally and C_{nkl} denoting expansion coefficients.

In order to convert results from effective exciton units to physical units, we need the effective mass and dielectric constant of the system under investigation. We will assume that screening is primarily due to the medium surrounding the CNT, and simply take it as a parameter $\epsilon \approx 3.5$ suitable for CNTs suspended in water or embedded in a zeolite crystal. As has been detailed in Ref. [3], the radius of *any* CNT is $R \approx 0.1$ exciton Bohr radii following from the inverse dependence of the effective masses on the physical CNT radius. Similarly, the exciton Rydberg is approximately $Ry^* \approx 0.21$ eV Å$/r$, with r indicating the CNT radius in Å.

B. π-electron tight-binding model

To extend upon the two-band effective mass model presented above, we apply a simple tight-binding π-electron model, which takes both multiple bands and the atomic geometry into account [26]. However, we neglect any response from σ electrons in addition to σ-π hybridization known to follow from the CNT curvature. The latter effect can be incorporated through the extended tight-binding scheme, and would explain, e.g., the full band gap/CNT diameter dependence [13]; however, this complication is known to affect the exciton binding energy very little [13]. In fact, the π electrons of conjugated carbon systems are known [26] to be well described within the semiempirical TB approximation, taking only nearest neighbor interaction into account and fitting TB parameters to a band structure derived from density functional theory. Following the formulation of Ref. [24], we expand the molecular TB orbitals in Bloch sums of the form

$$\chi_{\alpha k}(\vec{r}) = \frac{1}{\sqrt{N}}\sum_{n=1}^{N} e^{ikna}\phi(\vec{r} - \vec{r}_{\alpha n}), \quad (6)$$

where periodic boundary conditions have been introduced, essentially restricting the calculation to a ring consisting of N CNT unit cells, each of length a (note that all distances are measured along the CNT axial direction, and, hence, this is simply a consistent way of introducing k-space discretization). Here, $k = \pi(2p - N - 2)/(aN)$ is the Bloch wave number, with $p = 1,2,...,N$, while $\phi(\vec{r} - \vec{r}_{\alpha n})$ represent the αth π orbital inside the nth CNT unit cell. The full TB molecular orbital $\psi_{sk}(\vec{r})$ is then written as a linear combination of Bloch sums

$$\psi_{sk}(\vec{r}) = \sum_{\alpha} c_{\alpha sk}\chi_{\alpha k}(\vec{r}). \quad (7)$$

The expansion coefficients $c_{\alpha sk}$ and one-electron energies E_{sk} are found by diagonalizing the nonorthogonal nearest neighbor TB Hamiltonian [26], with the electrostatic field incorporated similarly to Ref. [16]. Taking the on-site energy for a $2p$ electron to $E_{2p} = -5$ eV, the hopping integral to $\gamma = -2.87$ eV, and the overlap integral to $s = 0.1$ yields π-electron band energies in good agreement with density functional theory. Thus, the band gap will be too small, requiring a quasiparticle correction which can be implemented in the simplest way using the scissors approximation, leading to a simple shift of the conduction band energies by a suitable energy. An appropriate energy shift is found by comparing the calculated first excitonic absorption peak, at photon energy E_{11}, with the experimentally derived data of Ref. [20].

Following Ref. [24], the exciton states Ψ_n are expanded in terms of singly excited Slater determinants $|(vk) \rightarrow (ck)\rangle$, constructed by replacing a valence band state with a conduction band state of identical wave number in the TB ground state Slater determinant. Hence, $\Psi_n = \sum_{cvk} A_{kvc}^{(n)}|(vk) \rightarrow (ck)\rangle$. This leads to the Bethe-Salpeter equation, yielding the expansion coefficients $A_{kvc}^{(n)}$,

$$\sum_{k'v'c'}[2V_{kvc,k'v'c'} - W_{kvc,k'v'c'}]A_{k'v'c'}^{(n)} = [\tilde{E}_n - E_{ck} + E_{vk}]A_{kvc}^{(n)}. \quad (8)$$

Here $\tilde{E}_n$ denotes the nth exciton energy while $W_{kvc,k'v'c'}$ and $V_{kvc,k'v'c'}$ denote the screened Coulomb matrix element and the unscreened exchange matrix element, respectively. These are calculated in a manner identical to Ref. [24]. For the Coulomb matrix elements, we apply the same screening constant as in the Wannier model $\epsilon_c = 3.5$; however, due to the truncated electron basis, it is necessary [24] to include a phenomenological screening of $\epsilon_x = 2$ of the exchange interaction due to the neglected σ electrons and the surrounding medium to achieve agreement with experiments. Hence, we apply a Coulomb interaction kernel regularized using the Ohno-form [5,24] $V_i(r) = U[1 + (Ur/q_c)^2]^{-1/2}/\epsilon_i$. Here, r indicates electron-hole separation, $q_c = e^2/(4\pi\epsilon_0)$, $i \in \{c, x\}$ (indicating "Coulomb" and "exchange," respectively), and $U = 20.08$ eV is the Ohno parameter [24].

C. Optical properties and intrinsic lifetimes

Having calculated a set of exciton states and energies by Eq. (8), the optical response may be evaluated using the well-known expression for the diagonal elements of the dielectric tensor derived from first order time-dependent perturbation theory [24]:

$$\epsilon_{aa}(\omega) = 1 + \frac{2e^2\hbar^2}{\epsilon_0 m^2 \Omega} \sum_n \frac{|\vec{P}_n \cdot \hat{a}|^2}{E_n[E_n^2 - \hbar^2(\omega + i\Gamma)^2]}, \quad (9)$$

where m is the electron mass, Ω is the CNT volume defined as in Ref. [27], Γ is a phenomenological dampening factor, and a is a Cartesian index with z aligned along the CNT long axis while $\hat{a}$ represents the corresponding unit vector. Also, $\vec{P}_n = \langle 0|\hat{\vec{P}}|n\rangle = \sum_{cvk} A_{kvc}^{(n)} \vec{p}_{vc}(k)$ is a momentum matrix element coupling the nth excited state to the ground state. The one-electron momentum matrix element between the conduction band c and valence band v at k in reciprocal space $\vec{p}_{vc}(k)$ may be calculated according to Ref. [28]. Furthermore, the exciton states possess an intrinsic radiative decay rate, which may be written according to a one-dimensional Einstein formula [6,7]

$$\gamma_n = \frac{e^2|\vec{P}_n \cdot \hat{z}|^2}{2\epsilon_0 \hbar m^2 c^2 L}, \quad (10)$$

where $L = Na$ is the length of the CNT. Note that we may restrict the analysis to decay from axially (z) polarized excitons due to depolarization effects [6,7]. In the tight-binding model, we have access to all parameters and variables entering in Eqs. (9) and (10); however, in the Wannier model the exciton momentum matrix elements are not known. To avoid this problem, we may apply the following approximation [24]: $|P_n \cdot \hat{a}|^2 \approx 2L|\vec{p}_{vc} \cdot \hat{a}|^2 |\langle \Psi_n(0, \theta_e, \theta_h)\rangle_{\theta_e = \theta_h}|^2$, where $\vec{p}_{vc}$ (approximated as k independent in the Wannier model) is the momentum matrix element coupling the valence band v and conduction band c used to construct the Wannier exciton. The brackets $\langle\rangle_{\theta_e = \theta_h}$ indicate the angular average over θ_e while fixing $\theta_h = \theta_e$. Furthermore, in the effective mass model, we take the one-electron matrix elements p_{vc} to be independent of the electrostatic field strength, and calculate the decay rates relative to the value found for a vanishing electrostatic field γ_0. Hence, $\gamma_n/\gamma_0 \approx |\langle \Psi_n(0, \theta_e, \theta_h)\rangle_{\theta_e = \theta_h}/\Psi_n^{(0)}(0, 0, 0)|^2$ with $\Psi_n^{(0)}$ indicating the exciton wave function calculated for $F = 0$.

In a typical experiment, the exciton recombination rates may be probed by measuring the nanosecond-scale time evolution of the photoluminescence (PL) generated by CNTs excited with femtosecond pulses [25]. Since the excited electron-hole pairs thermalize rapidly compared to radiative decay paths [6,7,25], the measured PL is generated by a statistically occupied ensemble of exciton states, some of which are *dark* (i.e., are optically inactive). Hence, in order to compare our theoretical results directly with, e.g., time-resolved PL experiments, we have to take the thermal average along the lines presented in Refs. [6,7]. In general terms, the full exciton ensemble may be indexed by an exciton band index n and a wave vector index Q (in addition to spin indices, however, we do not include relaxation processes involving spin flips in the present work). Hence, the thermal average should be taken over both of these indices. Spataru *et al.* [6] have derived a simple expression for the effective radiative decay rate, taking into account the four lowest singlet states (of which only a single bright exciton is assumed), and taking the excitonic states to follow a parabolic dispersion in Q. We here generalize their method slightly to not depend on a specific exciton fine structure, describing this information through E_n and γ_n instead:

$$\gamma_{\text{eff}}(T) = \frac{\sum_n \gamma_{\text{eff}}^{(n)}(T) e^{-E_n/k_B T}}{\sum_n e^{-E_n/k_B T}}. \quad (11)$$

Here, $\gamma_{\text{eff}}^{(n)} = 4/3\gamma_n\sqrt{\Delta/(\pi k_B T)}$ is the effective radiative recombination rate of the nth exciton band at temperature T taking into account the thermal Q average of the exciton band [6]. Note that E_n and γ_n are evaluated at $Q = 0$. While a relatively broad range of the band is thermally occupied, only the bottom $[E_n; E_n + \Delta], \Delta = E_n^2/(2c^2 M)$ energy interval allows for coupling to the radiation field, significantly reducing the effective recombination rate of the Q-averaged nth band, when compared to γ_n. Here, $M \approx m_e + m_h$ indicates the effective electron-hole center mass, where m_e and m_h are the effective masses of individual electron and hole bands.

III. RESULTS AND DISCUSSION

The electron and hole, being oppositely charged quasiparticles, are effectively separated due to the electrostatic field. Considering the angular distribution of the electron-hole wave function for an $R = 0.5$ Wannier exciton plotted for $z = 0$ in Fig. 1, three distinct phases may be observed:

(i) With vanishing electrostatic field, the exciton complex displays no dependence on the center of mass coordinate, although Coulomb attraction tends to localize the hole around the electron (and vice versa). Hence, the exciton wave function has a constant maximum on the $\theta_e = \theta_h$ diagonal, illustrated by the dashed lines in Fig. 1. (ii) In an intermediate regime, with larger electrostatic field, the electron-hole complex remains bound. However, the two-particle wave function displays the largest amplitude for polarized excitons at angular coordinates allowing slight separation of electron and hole, with the resulting dipole aligned along the electrostatic field. This results in the slight bulge of the wave function away from the $\theta_e = \theta_h$ diagonal near $\theta_e \approx \theta_h \approx \{0, \pi\}$. (iii) With large enough fields, the electron and hole may dissociate, occupying
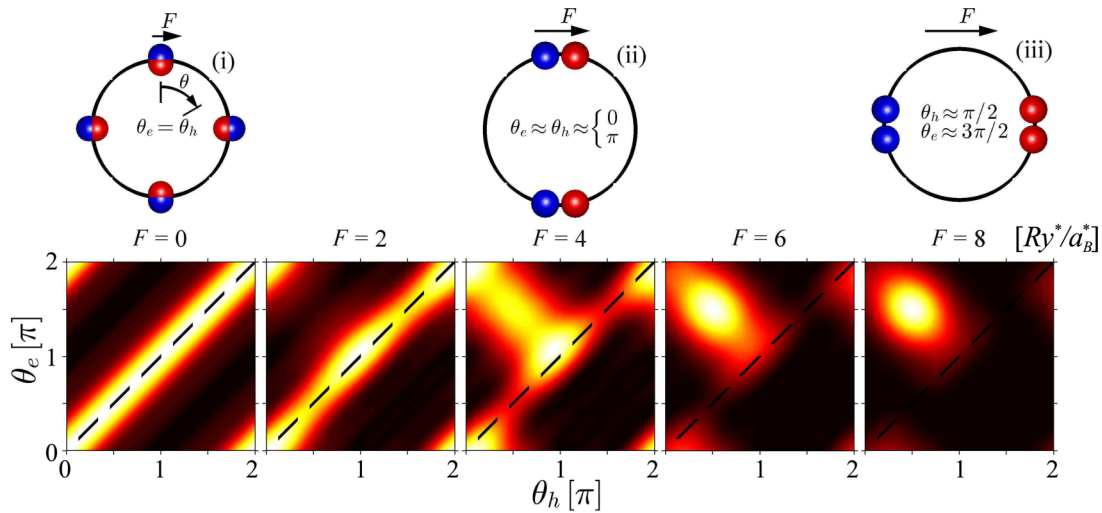
FIG. 1. (Color online) Absolute square of exciton wave functions at $z = 0$ for an $R = 0.5$ tube with increasing applied field strength F. Note that the electrostatic field is reported in effective exciton units Ry^*/a_B^*. The schematic illustrations indicate the electron (blue spheres) and hole (red spheres) configurations with largest wave function amplitude, and represent phases (i) to (iii) discussed in the text. Note that we draw multiple exciton complexes to indicate equivalent angular configurations; however, only two-particle interactions are taken into account (i.e., effects from trions, biexcitons, and the like are not included).

positions on opposite sides of the CNT. This configuration corresponds to a maximum exciton wave function when $\theta_e \approx 3\pi/2$ and $\theta_h \approx \pi/2$. However, if the CNT circumference is smaller than the typical electron-hole distance (i.e., smaller than the exciton Bohr radius), the electron and hole still overlap requiring much larger fields for complete dissociation. Note that to exaggerate effects of the electrostatic field, we have chosen in Fig. 1 a larger radius than is typical for a CNT, as has already been discussed. However, this result may be relevant for other nanotubular structures, which do not follow the peculiar band gap/effective mass scaling particular to CNTs.

In Fig. 2, we consider the electron-hole wave function, the exciton binding energy, and the radiative decay rate for an $R = 0.2$ tube predicted by the Wannier model. A dramatic drop in the decay rate results from the reduced electron-hole overlap, evident from the wave function plots of the same figure. Furthermore, the redshift of the bound exciton compares favorably with experimental results [22], which also demonstrate a redshift of the main E_{11} absorption peak quadratic in the applied electrostatic field. Similar results were obtained for electrostatically perturbed cylindrical quantum wells, where a Wannier model was applied by Wu and Tomić [29]. The general redshift of the exciton energies may be understood in the simple hydrogenic Stark picture. Here, the leading order energy correction of a two-particle Coulomb-attracted system due to a perturbing, uniform electrostatic field is indeed negative, and quadratic in field strength [30]. In simple terms, the redshift may be understood as the interaction energy of an induced dipole with the inducing field.

Within the TB exciton model, we have access to the excitation energy spectrum and exciton wave functions needed for evaluating the linear optical response for a range of applied electrostatic field strengths, and we plot results for a (20,0) CNT in Fig. 3. In the absence of an electrostatic field, the interband transitions, giving rise to the dispersion in the dielectric function of semiconducting CNTs, are subject to

a set of strict optical selection rules, which allow only one-electron transitions conserving angular momentum. Hence, the absorption edges for the axial (ϵ_{zz}) and the transversal (ϵ_{xx}) dielectric functions differ in the one electron picture [8]—an effect which is also observed when including excitons [31], as may be verified by comparing Figs. 3(a) and 3(b). In Fig. 3(a), the results for a vanishing electrostatic field (black curves) display two main peaks corresponding to the so-called E_{11} and E_{22} excitons. The applied scissor shift ensures that we find $E_{11} = 0.68$ eV, in agreement with experimentally derived
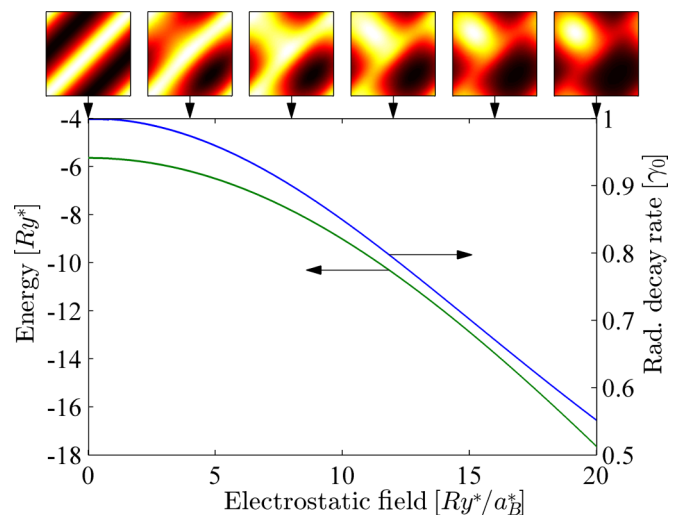
FIG. 2. (Color online) Excitonic lifetimes and energies calculated using the effective mass Wannier model for an $R = 0.2$ tube. Lifetimes are normalized to the case of a vanishing electrostatic field, while energies are displayed in effective exciton Rydbergs and are measured relative to the unperturbed band gap energy. Top panels display the electron-hole wave functions at electrostatic fields indicated by the arrows. The axes of the respective top panels are identical to the ones in Fig. 1.
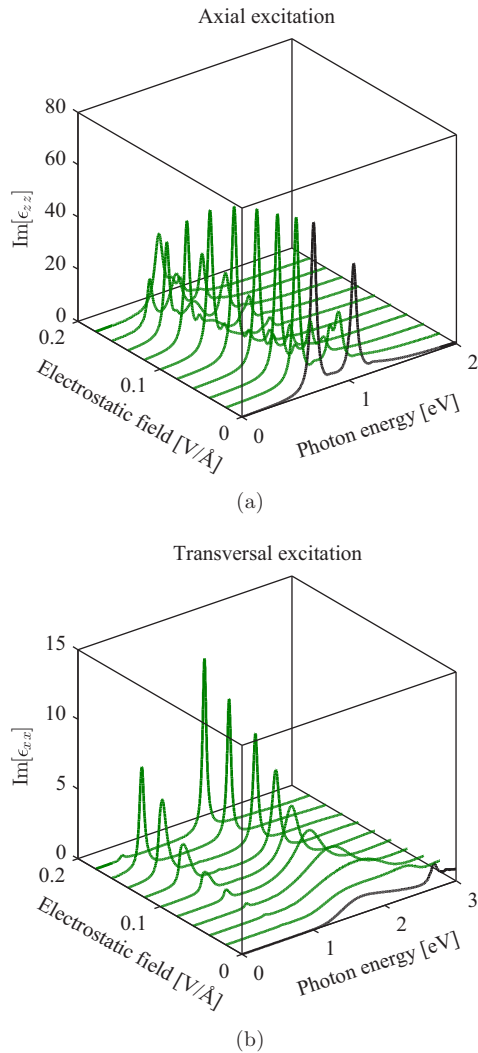
FIG. 3. (Color online) Imaginary part of the dielectric function for a (20,0) CNT with the exciting optical field aligned (a) parallel to the axial direction of the CNT and (b) perpendicular to this direction. The black lines indicate the response at a vanishing applied electrostatic field.

results reported by Weisman and Bachilo [20]. However, we model $E_{22} = 1.04$ eV, i.e., approximately 7% smaller than reported by Weisman and Bachilo. This disagreement, however, is well within the error introduced by, e.g., our simplified screening model or the neglected energy dependence of the quasiparticle correction. For large tubes, the scaling rule $E_{22}/E_{11} \approx 1.7$ applies reasonably well [20,32,33]. Experimental results suggest that [20] $E_{22}/E_{11} = 1.63$ for a (20,0) CNT while we find a slightly lower $E_{22}/E_{11} = 1.54$ due to the underestimation of E_{22}.

The result for transversal excitation polarization and vanishing electrostatic field is displayed as the black curve in Fig. 3(b). Here, a relatively broad, featureless peak dominates the absorption edge instead of the narrow features typical for strongly bound electron-hole pairs found for axial excitations. Previous studies [34] have demonstrated how inclusion of electron-electron Coulomb interaction may lead to quenching of the oscillator strength of the transversely excited excitons in CNTs due to so-called depolarization effects. The exchange

interaction is particularly important in this context [34] and, indeed, we recover a transversal spectrum dominated by narrow excitonic features when taking this term to vanish (i.e., by taking the limit $\epsilon_x \to \infty$). Hence, we conclude that the optical signatures of transversally excited excitons are much weaker than longitudinal ones. Furthermore, from a one-electron TB theory, the lowest transversally allowed optical excitation is expected at a photon energy $E_{12} \approx (E_{11} + E_{22})/2$; however, depolarization effects are known to result in transversal peaks close to and below [35] E_{22}, in agreement with our calculations.

Upon applying the electrostatic field, the cylindrical symmetry is broken, which lifts the optical selection rules. This results, e.g., in a new, otherwise forbidden, absorption peak developing in the transversal dielectric function near energies which correspond to the lowest E_{11} transition in the axial spectrum. For the case of a (20,0) CNT, this peak may be seen at 0.52 eV in Fig. 3(b). Dramatic changes of the spectral shapes of various peaks are also observed, with features in the transversal spectrum becoming much narrower and increasing in intensity. For example, a sharp peak appears in the transversal spectrum [Fig. 3(b)] at photon energies near 1.75 eV and electrostatic fields near 0.15 V/Å. The exact origin of changes induced in higher-lying spectral features is a combination of exciton energy shifts, broken cylindrical selection rules, and reshuffled oscillator strengths. Hence, such features are difficult to interpret in simple terms, using, e.g., a two-band Wannier model, requiring instead more complicated numerical simulations, such as the TB model applied here.

A plot of the excitation energies and decay rates of the lowest ten excitons, displayed in the middle and lower panels of Fig. 4, allows a more detailed analysis of this behavior. It is apparent that some of these states are dark, i.e., they are associated with a vanishing optical matrix element P_n and, hence, a vanishing radiative decay rate. The existence and analysis of such dark excitons in terms of symmetry has been reported before [13], and their optical inactivity represent a manifestation of the mentioned angular momentum single-particle selection rules in the exciton picture. Hence, from the middle panels of Fig. 4, it may be verified how optical selection rules are broken with the application of an electrostatic field, causing a few dark excitons to become bright, with nonvanishing decay rates. Also, the decay rates of all states are seen to be modulated strongly by the electrostatic field, in good agreement with the results predicted using the effective mass model. However, the Wannier model does not contain the atomic resolution necessary to distinguish between dark and bright states, instead modeling only the behavior of the lowest bright exciton. In Figs. 4(a) and 4(b), we compare the relatively large (20,0) CNT with a smaller (7,0) CNT, and from that figure it may be verified that effects of exciton dissociation are more dramatic for the case of larger tubes, which allow more effective separation of the hole and electron. Also, the excited states are seen to redshift with the applied electrostatic field, with a pronounced splitting of degenerate excitation energies for large fields. This, in turn, has a dramatic impact on the optical spectra, displayed in the top panels of Figs. 4(a) and 4(b) and in Fig. 3. There, the main absorption peak is seen to redshift correspondingly, while a pronounced splitting of this peak is also observed.
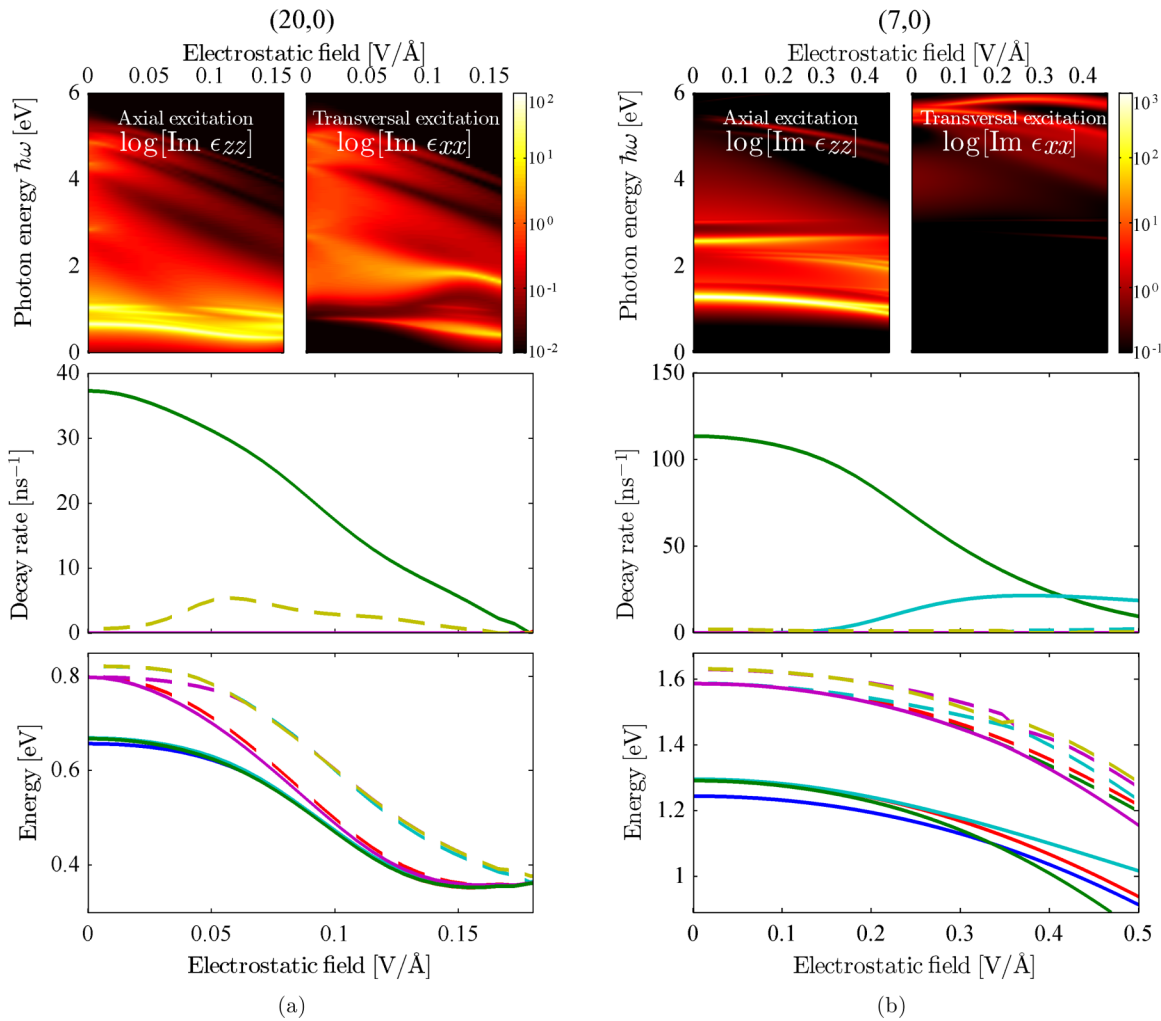
FIG. 4. (Color online) Logarithm of the imaginary part of the dielectric functions, radiative decay rates, and excitation energies of the ten lowest excitons found using the TB exciton model for a (a) (20,0) CNT and a (b) (7,0) CNT . We note that the top panels indicating the optical response display the same data as Figs. 3(a) and 3(b); however, here represented on a logarithmic scale to highlight the weak features. Please note that the line types (color/full/dashed) used in the middle and lower panels are identical, and indicate the respective exciton states.

Upon performing the statistical averaging in Eq. (11), we arrive at an effective decay rate for comparison with experiments [25], and we include the results for a (7,0) CNT and a (20,0) CNT in Fig. 5. Generally, the effective decay rates calculated for vanishing electrostatic fields correspond to lifetimes in the 10 ns range, in good agreement with both previous theory [6,7] and experiments [25]. Simply put, the reduction of the effective radiative decay rates by two orders of magnitude compared to the intrinsic decay rates, predicted by Eq. (10), is due to the thermal smearing of the excited electron-hole pair over an ensemble of exciton states, many of which fail to provide radiative recombination channels (i.e., they are dark). In fact, in the absence of an electrostatic field, the lowest exciton will be dark for any semiconducting CNT [6], followed by a bright exciton at slightly larger energy. This behavior may also be observed in Fig. 4. Hence, the statistical averaging [Eq. (11)] will occupy the dark states of lowest energy to a greater extent than the bright exciton, making the radiative decay less efficient. However, as is clearly evident from Fig. 4(b), the electrostatic field may close the gap between the lowest bright and dark states, thereby providing an
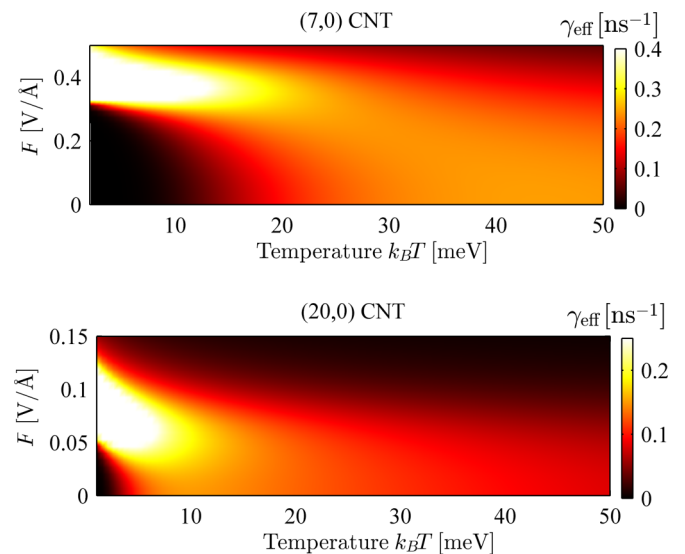
FIG. 5. (Color online) Effective radiative decay rates for a (7,0) CNT and a (20,0) CNT as a function of temperature and electrostatic field strength.
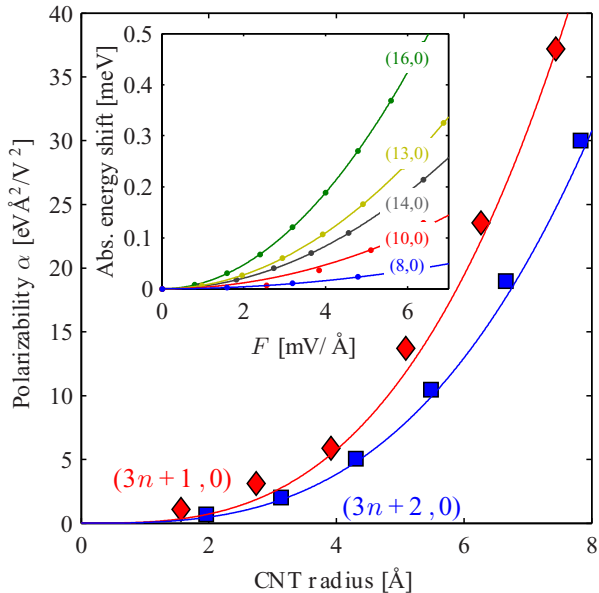
FIG. 6. (Color online) Systematic study of the low-field response for various CNTs. Only semiconducting tubes are considered, hence all members of the $(3n,0)$ CNT family are excluded (n indicating an integer). The lines represent a power law fit $\alpha = \beta r^3$, with r indicating the CNT radius, while β is given by 0.09 and 0.06 eV/V^{2}Å for the $(3n + 1,0)$ and $(3n + 2,0)$ families, respectively. The inset displays a selection of the fits used for extracting the polarizabilities (lines) and the shifts calculated using the full TB model (dots).

efficient radiative decay channel. The transition field strength, where the lowest dark and bright states become degenerate, is found at 0.33 and 0.12 eV/Å for the (7,0) and the (20,0) CNTs, respectively. In Fig. 5, a clear signature of this is observed at low temperatures, where a dramatic increase in the effective radiative decay rate is observed near these field strengths. However, a further increase of the electrostatic field tends to reduce the intrinsic decay rates, as displayed in Fig. 4, which eventually reduces the effective rates. At higher temperatures, effects of closing the gap between the first dark and bright excitons are less pronounced due to the increased thermal smearing resulting from averaging over a wider distribution of decay channels.

The redshift with applied electrostatic field is nearly quadratic in the low-field limit. Hence, we may approximate the energy shift ΔE by the formula $\Delta E \approx -\alpha/2 \, F^2$, and then proceed to fit the polarizability α for various CNT species. We display the result in Fig. 6. There, we consider the redshift of the bright exciton (under axial excitation) having lowest energy. The inset illustrates the fitted functions (lines) compared to shifts calculated using the full TB model (dots), and indeed shows very good agreement. The extracted values of α are displayed in the main figure, where an increasing sensitivity of larger tubes to the applied electrostatic field may be observed. Note that we only consider semiconducting tubes in this work. In the limit of electrostatic fields representing a perturbation

energy comparable to the band gap, a semiconductor-metal transition has been reported [2]. Since metallic species are described by photophysics more involved than the model applied in this work (metallic screening, etc.), the limit of very large tubes cannot be taken due to the inverse dependence of the band gap on tube radius. Hence, for very large tubes even small fields will cause a semiconductor-metal transition, invalidating the present model for that case. Thus, the fitted α values may not be extrapolated to infinitely large tubes either. We can compare our theoretical results in Fig. 6 directly with the experiments displayed in Fig. 4(b) of Ref. [22]. The experimentally reported values for α are larger by a factor of 100 compared to our calculations; however, this discrepancy is easily explained by the fact that the electrostatic field in the experiments are aligned primarily along the long axis, which is more easily polarized. To compare with our results, it would be interesting to perform similar experiments, with the electric field polarized primarily transversally to the tube axis.

Comparing with previous theoretical work on CNTs influenced by electrostatic fields, such as Refs. [2,14,15], we conclude that the one-electron models applied there are indeed insufficient for correctly reproducing electro-optic effects in CNTs, mainly due to the dominance of bound electron-hole pairs. Hence, features such as modulation of line shapes, redshift of absorption peaks, and transfer of oscillator strength due to the electrostatic fields are all affected strongly by inclusion of electron-hole attraction. These conclusions are in good agreement with previous studies on the similar case of electrostatic fields applied along the CNT tube axis [12].

IV. CONCLUSION

In conclusion, we demonstrate that applying an electrostatic field across a CNT can have a dramatic impact on its excitonic energy spectrum, with a general redshift of the lowest lying excitons. This is a result of increasingly polarized excitons, where the exciton and hole wave functions become separated. With stronger applied fields, this results in delocalized excitons where the electron and hole are located on opposite sides of the CNT. This trend is accompanied by a dramatic drop in the radiative exciton recombination rates due to reduced overlap between electrons and holes. However, a statistical averaging procedure, taking into account the thermal occupation of the exciton states, reveals that introducing a strong electrostatic field may increase the effective recombination rate seen in experiments at low temperatures. Hence, we demonstrate theoretically the possibility of tuning the excitonic optical response of CNTs by an electrostatic field in a geometry, which may be realized experimentally.

[1] J. O'Keeffe, C. Wei, and K. Cho, Appl. Phys. Lett. **80**, 676 (2002).

[2] Y. Li, S. V. Rotkin, and U. Ravaioli, Nano Lett. **3**, 183 (2003).

[3] T. G. Pedersen, Phys. Rev. B **67**, 073401 (2003).

[4] T. G. Pedersen, Carbon **42**, 1007 (2004).

[5] V. Perebeinos, J. Tersoff, and P. Avouris, Phys. Rev. Lett. **92**, 257402 (2004).

[6] C. D. Spataru, S. Ismail-Beigi, R. B. Capaz, and S. G. Louie, Phys. Rev. Lett. **95**, 247402 (2005).

[7] V. Perebeinos, J. Tersoff, and P. Avouris, Nano Lett. **5**, 2495 (2005).

[8] A. Zarifi and T. G. Pedersen, Phys. Rev. B **74**, 155434 (2006).

[9] M. Y. Sfeir, T. Beetz, F. Wang, L. Huang, X. M. H. Huang, M. Huang, J. Hone, S. O'Brien, J. A. Misewich, T. F. Heinz, L. Wu, Y. Zhu, and L. E. Brus, Science **312**, 554 (2006).

[10] T. S. Li and M. F. Lin, Nanotechnol. **17**, 5632 (2006).

[11] M. S. Dresselhaus, G. Dresselhaus, R. Saito, and A. Jorio, Annu. Rev. Phys. Chem. **58**, 719 (2007).

[12] V. Perebeinos and P. Avouris, Nano Lett. **7**, 609 (2007).

[13] J. Jiang, R. Saito, G. G. Samsonidze, A. Jorio, S. G. Chou, G. Dresselhaus, and M. S. Dresselhaus, Phys. Rev. B **75**, 035407 (2007).

[14] T. H. Cho, W. S. Su, T. C. Leung, W. Ren, and C. T. Chan, Phys. Rev. B **79**, 235123 (2009).

[15] J. D. Correa, C. G. Rocha, A. Latgé, and M. Pacheco, J. Phys.: Condens. Matter **23**, 065301 (2011).

[16] M. L. Trolle and T. G. Pedersen, J. Phys.: Condens. Matter **25**, 325301 (2013).

[17] E. Verdenhalven and E. Malić, J. Phys.: Condens. Matter **25**, 245302 (2013).

[18] Q. H. Wang, K. Kalantar-Zadeh, A. Kis, J. N. Coleman, and M. S. Strano, Nat. Nano **7**, 699 (2012).

[19] T. F. Rønnow, T. G. Pedersen, and H. D. Cornean, Phys. Rev. B **81**, 205446 (2010).

[20] R. B. Weisman and S. M. Bachilo, Nano Lett. **3**, 1235 (2003).

[21] T. Takenobu, Y. Murayama, and Y. Iwasa, Appl. Phys. Lett. **89**, 263510 (2006).

[22] M. Yoshida, Y. Kumamoto, A. Ishii, A. Yokoyama, and Y. K. Kato, Appl. Phys. Lett. **105**, 161104 (2014).

[23] T. G. Pedersen and T. B. Lynge, Phys. Rev. B **65**, 085201 (2002).

[24] T. G. Pedersen, Phys. Rev. B **69**, 075207 (2004).

[25] A. Hagen, M. Steiner, M. B. Raschke, C. Lienau, T. Hertel, H. Qian, A. J. Meixner, and A. Hartschuh, Phys. Rev. Lett. **95**, 197401 (2005).

[26] R. Saito, G. Dresselhaus, and M. S. Dresselhaus, *Physical Properties of Carbon Nanotubes* (Imperial College Press, London, 1998).

[27] T. G. Pedersen and K. Pedersen, Phys. Rev. B **79**, 035422 (2009).

[28] T. G. Pedersen, K. Pedersen, and T. B. Kriestensen, Phys. Rev. B **63**, 201101(R) (2001).

[29] S. Wu and S. Tomić, J. Appl. Phys. **112**, 033715 (2012).

[30] N. Fröman and P. O. Fröman, *Stark Effect in a Hydrogenic Atom or Ion* (Imperial College Press, London, 2008).

[31] S. Kilina, S. Tretiak, S. K. Doorn, Z. Luo, F. Papadimitrakopoulos, A. Piryatinski, A. Saxena, and A. R. Bishop, Proc. Natl. Acad. Sci. USA **105**, 6797 (2008).

[32] S. M. Bachilo, M. S. Strano, C. Kittrell, R. H. Hauge, R. E. Smalley, and R. B. Weisman, Science **298**, 2361 (2002).

[33] C. L. Kane and E. J. Mele, Phys. Rev. Lett. **93**, 197402 (2004).

[34] H. Ajiki, J. Phys.: Condens. Matter **24**, 483001 (2012).

[35] Y. Miyauchi, M. Oba, and S. Maruyama, Phys. Rev. B **74**, 205440 (2006).